An ab Initio Three-Dimensional Torsion−Torsion−Bending Analysis of the Far Infrared Spectra of Dimethylamine

M. L. Senent*

Departamento de Química, Facultad de CyTA y C.Químicas, Universidad de Burgos, Plaza Misael Bañuelos, Burgos 09001, Spain

Y. G. Smeyers

I. Estructura de la Materia, C.S.I.C., Serrano 123, 28003 Madrid, Spain

D. C. Moule

Department of Chemistry, Brock University, St. Catharines, Ontario L2S3A1, Canada

Received: September 29, 1997; In Final Form: May 13, 1998

The frequencies of the three large amplitude modes of dimethylamine (DMA) were analyzed using a three-dimensional (3D) model, the independent variables of which are the two torsional angles and the CNC symmetric bending angle. For this purpose, the potential energy surface and the kinetic parameters of the vibrational Hamiltonian were determined using fully optimized ab initio calculations performed at the MP2/6-311G(d,p) and MP4/6-311G(d,p) levels on 150 nuclear conformations. The positions of the two first hot bands were also calculated. The three fundamentals, 255.4, 216.9, and 409.8 cm^{-1}, as determined with the MP4/6-311G(d,p) approximation, are in a good agreement with the experimental frequencies of 256.3, 219.4, and 383 cm^{-1}, respectively. Torsional frequencies were compared with those obtained from a previously published two-dimensional model. The calculations confirm that the 3D model is indispensable for obtaining accurate band separations for the two different torsional modes.

Introduction

In the most stable structure of the electronic ground state, dimethylamine (DMA) has a pyramidal geometry and can be classified according to the C_s symmetry point group (see Figure 1). This molecule presents four large amplitude vibration modes that confer the properties of nonrigidity. These vibrations are the internal rotation of the methyl groups, the hydrogen inversion of the amine group, and the CNC bending mode. The two methyl groups have been found to interact strongly during their rotation. In addition, the torsions may interact weakly with the CNC bending mode and with the inversion of the NH hydrogen.

The structures, barriers, and torsional frequencies of DMA have been considered in many papers.[1−14] The most relevant infrared (IR) and Raman spectra of DMA were recorded by Durig, Griffin, and Groner in 1977.[1] Their assignments are unusually complex because the two torsional modes a′ and a″ are active in the IR range. Both sets of transitions lie in the same region of the spectrum and result in bc-hybrid and a-type bands. In addition, the CNC bending fundamental band appears in the same region. The assignment of the transitions involving these modes requires a theoretical model that is powerful enough to accurately describe the relative positions of the observed bands.

In a previous paper,[14] we assigned the torsional spectra using two-dimensional (2D) calculations of the IR band frequencies and intensities. The spectroscopic parameters were determined from ab initio calculations at several nuclear conformations. The remaining coordinates were fully optimized in all the nuclear conformations to account in some way for the interactions with the other vibrational modes. This procedure has been employed for the analysis of the torsional spectra of a large set of nonrigid molecules; for examples, acetone,[15] biacetyl,[16] dimethylether, (DME)[17,18] dimethylsulfide,[19] 2-butene derivatives,[20] and methylamine.[21] In the case of DMA, the calculations were performed by using the MP2/RHF approximation and the following different basis sets: 6-31G(d,p), 6-311G(d,p), and 6-311G(df,p). A relatively good agreement between the theoretical and experimental values was achieved.

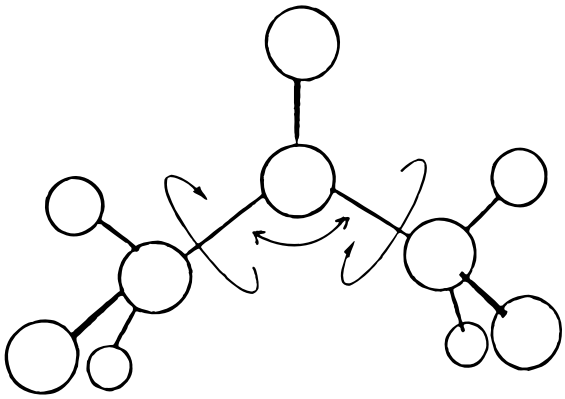

Figure 1. The molecular structure of dimethylamine, the torsional angles θ_1 and θ_2, and the bending angle β.

It may be inferred from this first DMA study[14] that the 2D model adequately describes the relative positions of the υ_{12} (a′) fundamental (000→010) and three first sequences (010→020; 020→030; 030→040), and the relative positions of the υ_{24} (a″) fundamental (000→100) and first sequence (100→200) of DMA. However, the 2D model is not powerful enough to treat the

S1089-5639(97)03145-9 CCC: $15.00
Published on Web 08/05/1998

relative band positions of these different modes. The observed separation between the two fundamentals is 36.9 cm^{-1}, whereas the calculated values with this restricted model are 27.5 cm^{-1} [MP2/6-31G(d,p)], 31.0 cm^{-1} [MP2/6-311G(d,p)], and 31.6 cm^{-1} [MP2/6-311G(df,p)].

The same behavior has been observed in DME,[17,18] which has been analyzed in 2D[17] and three dimensions (3D).[18] As in DMA, the 2D model does not reproduce the gap between the bands of the two different modes because the nonbonding interactions between the hydrogen atoms of the methyl groups are not explicitly employed. These interactions depend directly on the value of the COC angle. In 2D, the dependence on the barrier and the torsional interactions terms on the COC bending is parametric. In contrast, in 3D, the COC angle is an explicit coordinate and the dependence of the torsional terms on the bending is described in analytical form.

As a consequence, a significant improvement in the analysis of the torsional spectra may be expected by using three variables because the DMA and DME structures are comparable. The aim of the present paper is to analyze the torsional spectra of DMA with a 3D model where the CNC bending is explicitly considered as a third independent coordinate. The new frequencies are compared with those obtained in our previous paper[14] in 2D. Calculations are performed at the MP2/RHF and MP4/RHF levels using the 6-311G(d,p) basis set on 150 nuclear conformations. The Smeyers' formalism of the Group Theory for Non-Rigid Molecules[22,23] is employed to simplify the variational calculations.

Theory

The 3D vibrational Hamiltonian of DMA may be written as

$$H(\theta_1,\theta_2,\beta) = -\frac{\partial}{\partial\theta_1}B_{11}\frac{\partial}{\partial\theta_1} - \frac{\partial}{\partial\theta_2}B_{22}\frac{\partial}{\partial\theta_2} - \frac{\partial}{\partial\beta}B_{33}\frac{\partial}{\partial\beta} - \frac{\partial}{\partial\theta_1}B_{12}\frac{\partial}{\partial\theta_2} - \frac{\partial}{\partial\theta_2}B_{12}\frac{\partial}{\partial\theta_1} - \frac{\partial}{\partial\theta_1}B_{13}\frac{\partial}{\partial\beta} - \frac{\partial}{\partial\beta}B_{13}\frac{\partial}{\partial\theta_1} - \frac{\partial}{\partial\theta_2}B_{23}\frac{\partial}{\partial\beta} - \frac{\partial}{\partial\beta}B_{23}\frac{\partial}{\partial\theta_2} + V(\theta_1,\theta_2,\beta) \quad (1)$$

where $B_{ij}(\theta_1, \theta_2, \beta)$ represents the kinetic energy parameters and $V(\theta_1, \theta_2, \beta)$ is the 3D potential energy function that can be defined as the sum of the following three terms:

$$V(\theta_1,\theta_2,\beta) = V_{12}(\theta_1,\theta_2) + V^{\beta}(\beta) + V^{12\beta}(\theta_1,\theta_2,\beta) \quad (2)$$

The first term, $V^{12}(\theta_1, \theta_2)$, is a 2D energy function that depends on the two torsional angles, $V^{\beta}(\beta)$ is a one-dimensional (1D) function that depends on the CNC angle, and the last term, $V^{12\beta}$, describes the potential bending−torsion−torsion interactions.

The 3D dynamic model for DMA may be classified by the restricted nonrigid group[22,23] (r-NRG) that defines the nonrigid symmetry operations in terms of internal coordinates. This r-NRG group is identical to the group of symmetry operations that commute with the DMA nuclear Hamiltonian when the molecule is described as a 2D system[14] in which the variables are the torsional angles. Thus, the symmetry properties of the system remain unmodified by the addition of the bending motion as a third large amplitude coordinate. The r-NRG G_{18} group is defined by the same operations as those used in the 2D study of DMA. The G_{18} nonrigid group may be defined as

$$G_{18} = (C_3^I \times C_{3'}^I)\ \Lambda\ (WV)^I$$

where

$$C_3^I = [E + C_3 + C_3^2] \qquad (WV)^I = [E + WV]$$

where C_3 represents the 3-fold rotation of each methyl group. The term WV is simultaneously the double-switch and interchange operation and may be defined as

$$(WV)\ f(\theta_1,\theta_2,\beta) = f(-\theta_2,-\theta_1,\beta)$$

The V^{12} term of the potential may be developed by using a symmetry-adapted double Fourier series (i.e., the expansion coincides with that used in the 2D analysis of DMA):

$$V^{12}(\theta_1,\theta_2) = A_{000}^{cc} + \sum_{L>KK=0}^{2}\sum A_{LK0}^{cc}(\cos 3L\theta_1 \cos 3K\theta_2 + \cos 3K\theta_1 \cos 3L\theta_2) + \sum_{K=1}^{2} A_{KK0}^{cc}(\cos 3K\theta_1 \cos 3K\theta_2) + A_{110}^{ss} \sin 3\theta_1 \sin 3\theta_2 + \sum_{K=0}^{2} A_{1K0}^{cs}(\cos 3K\theta_1 \sin 3\theta_2 - \sin 3\theta_1 \cos 3K\theta_2) \quad (3)$$

In this expansion, the first seven terms transform as the totally symmetric representations of the G_{18} and the G_{36} group. The terms are symmetric with respect to the interchange (W), double switch (V) and double switch and interchange operations (WV). The additional three terms arise from the pyramidal nonplanar structure of DMA and transform as the totally symmetric representation of the G_{18} group.

The potential energy function for the CNC bending may be described by a Taylor series. The maximum of energy corresponds to the linear structure where CNC> = 180°. Because the barrier is extremely high, the lowest vibrational energy levels may be calculated by considering a single well, and the potential can be described by a Taylor series depending on the β angle where $\beta = \Delta(\text{CNC}>)$. $\beta = 0°$ corresponds to the minimum energy structure.

$$V^{\beta}(\beta) = \sum_{M=1}^{N} A_{00M}^{cc}\beta^M \quad (4)$$

Finally, the torsion−torsion−bending interactions terms are:

$$V^{12\beta}(\theta_1,\theta_2,\beta) = \sum_{L>KK=LM=1}^{2}\sum\sum^{N} A_{LKM}^{cc}\beta^M(\cos 3L\theta_1 \cos 3K\theta_2 + \cos 3K\theta_1 \cos 3L\theta_2) + \sum_{K=1M=1}^{2}\sum^{N} A_{KKM}^{cc}\beta^M (\cos 3K\theta_1 \cos 3K\theta_2) + \sum_{M=1}^{N} A_{11M}^{ss}\beta^M \sin 3\theta_1 \sin 3\theta_2 + \sum_{K=0M=1}^{2}\sum^{N} A_{1KM}^{cs}\beta^M(\cos 3K\theta_1 \sin 3\theta_2 - \sin K\theta_1 \cos 3K\theta_2) \quad (5)$$

The energy levels may be calculated variationally by developing the solutions on some basis set. For this purpose, the symmetry eigenvectors, which factorize the Hamiltonian matrix into blocks according to the irreducible representations of the G_{18} r-NRG, are used. These symmetry eigenvectors are obtained by projection of products of solutions of the double free rotor and the harmonic oscillator:

TABLE 1: Total Energies of Dimethylamine (cm^{-1})

θ_1'	θ_2'	β	MP2/TZ[a]	MP4/TZ[a]	θ_1'	θ_2'	β	MP2/TZ[a]	MP4/TZ[a]
0	0	0	40.66	41.82	0	0	5	210.85	220.21
60	0	0	1242.97	1203.42	60	0	5	1313.36	1291.86
60	60	0	2574.67	2493.15	60	60	5	2374.05	2326.93
30	0	0	763.86	748.14	30	0	5	829.17	828.48
60	30	0	1681.15	1621.71	60	30	5	1682.78	1644.75
30	30	0	1190.23	1154.73	30	30	5	1272.66	1253.43
30	−30	0	1563.56	1531.08	30	−30	5	1419.59	1413.64
0	30	0	425.66	407.03	0	30	5	603.21	594.28
30	60	0	2066.36	2011.24	30	60	5	1945.04	1919.13
−30	30	0	852.72	815.32	−30	30	5	950.72	925.79
0	0	3	99.92	106.39	0	0	−5	269.15	258.77
60	0	3	1239.14	1210.63	60	0	−5	1605.63	1544.49
60	60	3	2396.36	2336.39	60	60	−5	3329.24	3209.25
30	0	3	758.19	751.10	30	0	−5	1118.08	1082.52
60	30	3	1629.69	1583.25	60	30	−5	2174.31	2089.62
30	30	3	1194.12	1168.56	30	30	−5	1534.01	1478.72
30	−30	3	1426.05	1410.07	30	−30	−5	2189.51	2124.33
0	30	3	487.81	475.25	0	30	−5	662.90	630.48
30	60	3	1942.99	1906.11	30	60	−5	2667.39	2580.02
−30	30	3	860.49	830.15	−30	30	−5	1235.43	1180.66
0	0	−3	124.30	118.40					
60	0	−3	1402.34	1349.91					
60	60	−3	2952.26	2847.83					
30	0	−3	920.05	891.76					
60	30	−3	1910.54	1836.46					
30	30	−3	1339.32	1291.28					
30	−30	−3	1874.14	1822.80					
0	30	−3	512.26	484.98					
30	60	−3	2362.15	2287.77					
−30	30	−3	1017.58	969.52					

[a] MINIMUM: $(\theta_1', \theta_2', \beta) = (4.0, -4.0, 111.369)°$; E_{min} (MP2) = −134.829333 au; E_{min} (MP4) = −134.887942 au.

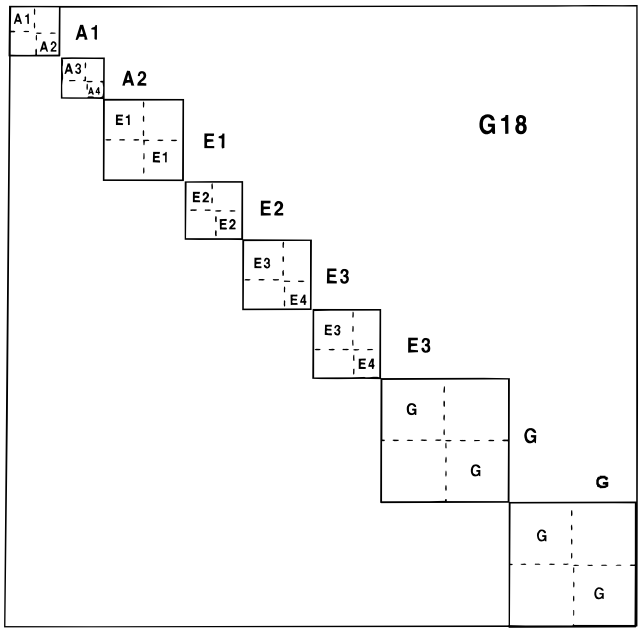

Figure 2. The Hamiltonian matrix factorized into the G_{18} and G_{36} (dotted line) irreducible representations.

$$\Phi(\theta_1,\theta_2,\beta) = \sum_I \sum_J \sum_N [C^{cc}_{IJN} X_N \cos I\theta_1 \cos J\theta_2 + C^{cs}_{IJN} X_N \cos I\theta_1 \sin J\theta_2 + C^{sc}_{IJN} X_N \sin I\theta_1 \cos J\theta_2 + C^{ss}_{IJN} X_N \sin I\theta_1 \sin J\theta_2] \quad (6)$$

where

$$X_N = H_{\gamma\beta} \exp(-\gamma^2\beta^2/2) \quad (7)$$

where $H_{\gamma\beta}$ represents the Hermite polynomials and

$$\gamma = \frac{A^{cc}_{002}}{B_{33}(0,0,0)} \quad (8)$$

Each symmetry eigenvector is the product of a torsional vector and a (even or odd) solution of the harmonic oscillator. The torsional symmetry eigenvectors may be also obtained from the set defined for the analysis of the acetone internal dynamics.[24] The G_{18} group of DMA is indeed a subgroup of the G_{36} group. Two sets of vectors from acetone form a single set of vectors for a single representation of DMA. In Figure 2, the Hamiltonian matrix is factorized in boxes according to the G_{18} and G_{36} representations. In this figure, the correlation between the representations of these two r-NRG groups is also illustrated.

The G_{18} group possesses two nondegenerate representations (A_1 and A_2) and one two-degenerate (E_3) representation. The representations E_1, E_2 and the two G components, G_1 a G_2, are pseudo-degenerate and each contains two inseparable representations. The IR and Raman selection rules coincide with those obtained in the previous 2D analysis of the DMA spectra.[14]

Computational Details

The 3D potential energy function was determined from the electronic energies of 150 selected nuclear conformations. Calculations were performed at the MP2/RHF and the MP4//MP2 levels by using the Gaussian 92 program.[25] All of the structures were fully optimized at the MP2/RHF levels with the 6-311G(d,p)(TZ) basis set. In this way, some interactions with the remaining vibration modes are taken into account.

Symmetry and energy criteria were applied in the selection of the nuclear conformations for the torsional coordinates (θ_1,θ_2) and the bending coordinate (β), respectively. With $\theta_1' = 0°$ and $\theta_2' = 0°$, one of the hydrogen atoms of each methyl group lies on the CNC plane pointing in the outward direction (see

TABLE 2: Expansion Coefficients of the Potential Energy Hypersurface (cm^{-1})

coefficient	MP2/TZ	MP4/TZ	coefficient	MP2/TZ	MP4/TZ
A^{cc}_{000}	1235.753	1198.354	A^{cc}_{220}	1.791	1.622
A^{cc}_{001}	−36.035	−31.788	A^{cc}_{221}	−0.366	−0.354
A^{cc}_{002}	9.030	8.882	A^{cc}_{222}	0.025	0.022
A^{cc}_{003}	−0.134	−0.137	A^{cc}_{223}	0.000	−0.001
A^{cc}_{004}	0.001	0.004	A^{ss}_{110}	−5.187	−5.309
A^{cc}_{100}	−659.930	−640.494	A^{ss}_{111}	12.889	12.665
A^{cc}_{101}	23.619	22.225	A^{ss}_{112}	−0.586	−0.564
A^{cc}_{102}	0.717	−0.714	A^{ss}_{113}	0.011	0.005
A^{cc}_{103}	0.015	0.015	A^{cs}_{010}	−42.672	−48.406
A^{cc}_{110}	36.116	36.072	A^{cs}_{011}	7.033	6.599
A^{cc}_{111}	−10.621	−10.157	A^{cs}_{012}	0.176	0.180
A^{cc}_{112}	0.398	0.395	A^{cs}_{013}	−0.003	−0.002
A^{cc}_{113}	−0.009	−0.013	A^{cs}_{110}	5.953	6.506
A^{cc}_{200}	20.851	19.648	A^{cs}_{111}	−0.546	−0.410
A^{cc}_{201}	−0.118	−0.042	A^{cs}_{112}	−0.066	−0.066
A^{cc}_{202}	0.005	0.008	A^{cs}_{113}	−0.001	−0.002
A^{cc}_{203}	−0.001	−0.001	A^{cs}_{210}	−2.368	−2.664
A^{cc}_{210}	2.857	3.255	A^{cs}_{211}	−0.425	−0.387
A^{cc}_{211}	0.310	0.240	A^{cs}_{212}	0.040	0.032
A^{cc}_{212}	−0.034	−0.031	A^{cs}_{213}	0.000	0.001
A^{cc}_{213}	0.002	0.003			

TABLE 3: Variation of the Torsional Barrier (cm^{-1}) with the Bending Angle[a]

	MP2/TZ		MP4/TZ	
β	$(V_{SP} - V_{min})$	$(V_{max} - V_{min})$	$(V_{SP} - V_{min})$	$(V_{max} - V_{min})$
−5	1394.6	3190.5	1344.2	3081.9
−3	1328.5	2944.3	1282.8	2847.3
0	1241.9	2628.3	1202.3	2549.0
3	1168.0	2366.3	1134.5	2304.3
5	1124.5	2216.2	1095.5	2165.1

[a] V_{max}, V_{sp}, and V_{min} are the energies corresponding to the values (60°, 60°, β), (60°, 0°, β) and (0°, 0°, β) of (θ_1, θ_2, β), respectively.

Figure 1). With this origin, the selected geometries were (0°, 0°), (60°, 0°), (60°, 60°), (30°, 0°), (0°, 30°), (30°, 60°), (60°, 30°), (30°, 30°), (30°, −30°), and (−30°, 30°). Conformations separated by 120° from this first set [i.e., (120°, 120°),... and (120°, −120°),..,] were also included in the fitting. Five values of the CNC angle around the CNC equilibrium value (β_0), were chosen for describing the variation of the energy with the bending angle. These angle values were $\beta = 0°, 3°, 5°, -3°, -5°$. The relative energies with respect to the most stable conformer were fitted to eq 2 using a least-squares algorithm and the SPSS program.[26] The 50 relative energy values of Table 1 were obtained from the fitted function. Table 2 shows the 41 expansion coefficients for this potential energy function.

In the most stable conformation, the methyl hydrogen atoms no longer lie in the CNC plane (where $\theta_1' = 0°$ and $\theta_2' = 0°$), but at $\theta_2' = -4.0°$. In the same way, the CNC angle was found to be 111.369° at the equilibrium geometry. It is necessary to remark that θ_1, θ_2, and β are the vibrational coordinates. The terms θ_1' and θ_2' were essentially introduced in the input of the ab initio calculations. Table 2 shows the expansion coefficients of the potential energy surfaces. The minima of these surfaces, $V = 0.0$ cm^{-1}, correspond to (θ_1, θ_2, β) = (0°, 0°, 0°), which is equivalent to (θ_1', θ_2', β) = (4.0°, −4.0°, 0°).

Table 3 shows the variation of the DMA torsional barrier $(V_{max} - V_{min})(\beta)$ and the effective barrier $(V_{sp} - V_{min})(\beta)$ with the bending coordinate β. V_{min}, V_{sp}, and V_{max} are the energies of the structures (θ_1, θ_2, β) = (0°, 0°, β), (θ_1, θ_2, β) = (60°, 0°, β) and (θ_1, θ_2, β) = (60°, 60°, β), respectively. The value of the barrier increases as the CNC angle decreases. The cos × cos ($A^{cc}_{11\beta}$) and the sin × sin ($A^{ss}_{11\beta}$) terms of the potential, which describe the interactions between the two methyl group torsions, also depend on the β coordinate. Figure 3 shows the variation of the torsional barrier, $(V_{max} - V_{min})(\beta)$, and the effective barrier, $(V_{spx} - V_{min})(\beta)$, with β. The two curves in Figure 4 represent the variation of $A^{cc}_{11\beta}$ and $A^{ss}_{11\beta}$ with β.

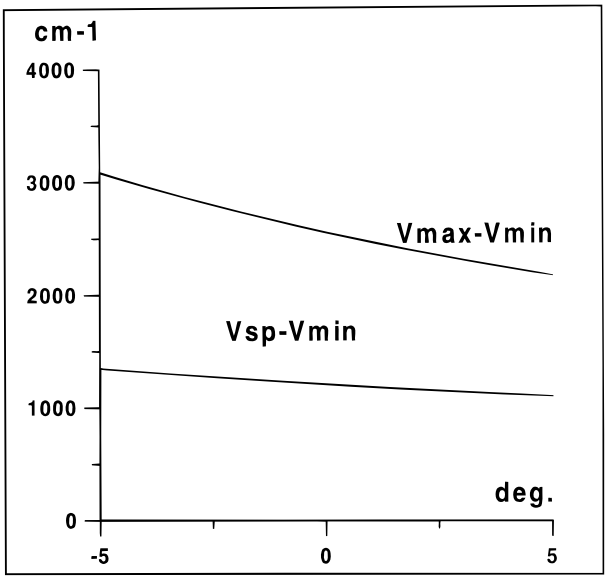

Figure 3. The variation of the barrier maximum, $(V_{max} - V_{min})$ and saddle points, $(V_{sp} - V_{min})$ as a function of the Δ(CNC) angle, β. β-(equilibrium) = 111.369°.

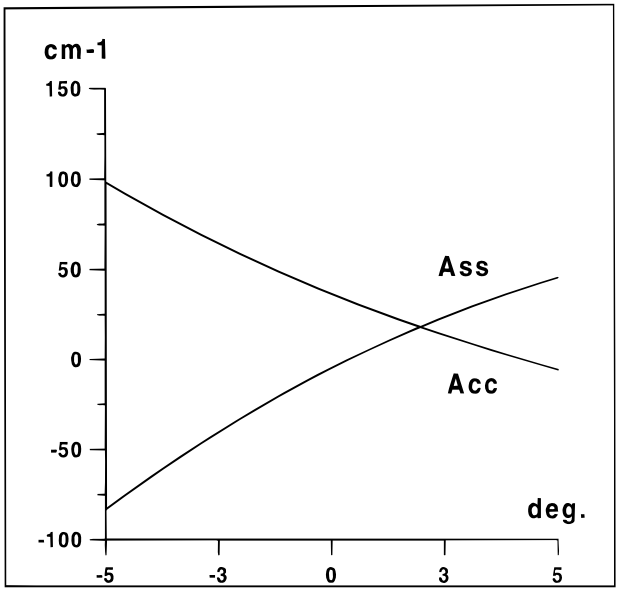

Figure 4. The $\sin(3\theta_1)\sin(3\theta_2)$ and $\cos(3\theta_1)\cos(3\theta_2)$ coupling terms as a function of the displacements of the CNC bending angle from equilibrium. $A^{SS} = -5.309 + 12.665\ \beta - 0.564\ \beta^2 + 0.005\ \beta^3$ and $A^{CC} = 36.072 - 10.157\ \beta + 0.395\ \beta^2 - 0.0013\ \beta^3$ (A^{SS} and A^{CC} in cm^{-1}; β in degrees).

The kinetic parameters for the Hamiltonian were determined with the numerical differentiation method described by Harthcock and Laane.[27] For this purpose, the G matrix was calculated numerically from the internal coordinates at the most stable structure. The MP2/6-311G(d,p) values were: $B_1 = B_2 = 6.5459$ cm^{-1}, $B_3 = 1.5911$ cm^{-1}, and $B_{12} = -1.0179$ cm^{-1}. In addition, $B_{12} = B_{13} = 0.0$, as a result of the orthogonality of the torsional and bending axes. The dependence of the kinetic operators on the remaining vibrational coordinates was not taken

TABLE 4: Dimethylamine Energy Levels[a]

v	v'	v''		MP4/TZ	MP2/TZ	v	v'	v''		MP2/TZ	MP4/TZ
0	0	0	A_1	447.19	442.54	0	0	1	A_1	854.45	852.34
			G	447.19	442.40				G	854.45	852.34
			E_1	447.19	442.54				E_1	854.45	852.34
			E_3	447.19	442.54				E_3	854.45	852.34
1	0	0	A_2	667.37	659.40	1	0	1	A_2	1071.69	1065.77
			G	667.37	659.40				G	1071.66	1065.73
			E_2	667.37	659.40				E_2	1071.64	1065.69
			E_3	667.37	659.40				E_3	1071.64	1065.69
0	1	0	A_1	705.31	697.98	0	1	1	A_1	1108.87	1107.05
			G	705.31	697.97				G	1108.82	1107.05
			E_1	705.31	697.97				E_1	1108.76	1106.97
			E_3	705.31	697.97				E_3	1108.76	1106.97
2	0	0	A_1	885.01	873.90	2	0	1	A_1	1280.16	1294.08
			G	885.02	873.91				G	1280.86	1294.81
			E_1	885.04	873.93				E_1	1281.64	1295.23
			E_3	885.04	873.93				E_3	1281.64	1295.23
1	1	0	A_2	913.70	902.75	1	1	1	A_2	1321.56	1311.61
			G	913.72	902.77				G	1321.83	1311.67
			E_2	913.74	902.80				E_2	1322.16	1311.76
			E_3	913.74	902.80				E_3	1322.16	1311.76
0	2	0	A_1	959.65	949.75	0	2	1	A_1	1361.91	1354.90
			G	959.66	949.76				G	1361.92	1354.89
			E_1	959.67	949.77				E_1	1361.94	1354.89
			E_3	959.67	949.77				E_3	1361.94	1354.89
3	0	0	A_2	1099.10	1085.46						
			G	1099.00	1085.35						
			E_2	1098.90	1085.24						
			E_3	1098.90	1085.24						
2	1	0	A_1	1117.51	1100.46						
			G	1117.30	1100.19						
			E_1	1117.10	1099.92						
			E_3	1117.10	1099.92						
1	2	0	A_2	1156.18	1142.50						
			G	1156.02	1142.31						
			E_2	1155.86	1142.12						
			E_3	1155.86	1142.12						
0	3	0	A_1	1209.11	1196.76						
			G	1209.08	1196.73						
			E_1	1209.05	1196.69						
			E_3	1209.05	1196.70						

[a] In cm^{-1}.

into account because our previous calculations[14] showed that they were approximately constant.

An accurate convergence of the lowest energy levels requires at least $37 \times 37 \times 10$ basis functions (37×37 solutions of the double rigid rotor and 10 harmonic oscillator solutions). This basis length implies a Hamiltonian matrix of the order 13 690. The symmetry conditions factorize this matrix into eight blocks of dimensions: $A_1(910)$, $A_2(780)$, G(3120), $E_1(1560)$, $E_2(1320)$, and $E_3(1440)$.

The Hamiltonian matrix was diagonalized using the Givens-Householder algorithm. The energy levels were classified according to their symmetries and the contribution of each harmonic oscillator solution to the 3D wave functions. The sixteen lowest levels are shown in Table 4. Each level splits into four microstates (A, E, E′, and G); that is, nine components corresponding to the nine equivalent wells on the potential energy surface. The levels in Table 4 are labeled by using the symmetry representations of the G_{18} r-NRG and the vibrational quantum numbers v and v' (for the torsions) and v'' (for the bending). The wave functions of the $v'' = 0$ levels depend largely on the lowest single harmonic oscillator solution, X_0. The most important contributions to the $v'' = 1$ wave functions are X_0 and X_1.Tables 5 and 6 show the frequencies corresponding to the cold bands (torsional transitions connecting $v'' = 0$ levels) and the hot bands (torsional transitions connecting $v'' = 1$ levels). Table 6 also gives the bending fundamental frequencies.

Assignments and Discussion

The frequencies of the cold bands, obtained in these 3D calculations (Table 5) can be compared with those determined in our first paper[14] using a 2D model at the same level of calculation. It is clear that the introduction of the third degree of freedom not only displaces the whole spectrum to higher wavenumbers, but it modifies slightly the relative positions of the transitions. In particular, the assignments are not changed. The observed displacements of the bands arise from the difference in the meaning of coordinates in the two models.

To understand this difference it is necessary to recognize that the 2D potential energy function cannot be represented by a planar surface corresponding to a single value of β on the 3D hypersurface. In the 3D model, the torsional parameters depend explicitly on β. In the 2D model, they depend parametrically on β, because the remaining 3N-6-2 internal coordinates are optimized. In particular, the CNC angle changes from 111.4 to 116.1° with the torsion. When the geometry is optimized, the CNC angle adjusts to minimize the interactions between the methyl groups. The relaxation of the bending coordinate decreases the torsional barrier and partially takes into account the potential interactions of the torsion with the bending.

It is impossible to compare the barriers obtained in the 2D and 3D models. In the 3D case, the barrier $(V_{max} - V_{min})(\beta)$ and the effective barrier $(V_{sp} - V_{min})(\beta)$ are functions of β

TABLE 5: Cold Band Positions for Dimethylamine (cm^{-1})

$v\,v'v'' \rightarrow$ v v′ v″		MP2/TZ	MP4/TZ	obs	calc − obs
	gearing mode				
0 0 0 → 0 1 0	$A_1 \rightarrow A_1$	258.12	255.44		
	$G \rightarrow G$	258.12	255.43	256.3	−0.9
	$E_1 \rightarrow E_1$	258.12	255.43		
	$E_3 \rightarrow E_3$	258.12	255.43		
0 1 0 → 0 2 0	$A_1 \rightarrow A_1$	254.34	251.77		
	$G \rightarrow G$	254.35	251.79	250.8	+1.0
	$E_1 \rightarrow E_1$	254.36	251.80		
	$E_3 \rightarrow E_3$	254.36	251.80		
0 2 0 → 0 3 0	$A_1 \rightarrow A_1$	249.46	247.01		
	$G \rightarrow G$	249.42	246.97	245.3	+1.7
	$E_1 \rightarrow E_1$	249.38	246.92		
	$E_3 \rightarrow E_3$	249.38	246.92		
0 3 0 → 0 4 0	$A_1 \rightarrow A_1$	243.46	241.16		
	$G \rightarrow G$	243.35	240.38	239.8	+0.6
	$E_1 \rightarrow E_1$	243.32	240.36		
	$E_3 \rightarrow E_3$	243.17	239.35		
1 0 0 → 1 1 0	$A_2 \rightarrow A_2$	246.33	243.35		
	$G \rightarrow G$	246.35	243.37	239.8	+3.6
	$E_2 \rightarrow E_2$	246.37	243.40		
	$E_2 \rightarrow E_3$	246.37	243.40		
	antigearing mode				
0 0 0 → 1 0 0	$A_1 \rightarrow A_2$	220.18	216.86		
	$G \rightarrow G$	220.18	216.86	219.4	−2.5
	$E_1 \rightarrow E_2$	220.18	216.86		
	$E_3 \rightarrow E_3$	220.18	216.86		
1 0 0 → 2 1 0	$A_2 \rightarrow A_1$	217.64	214.50		
	$G \rightarrow G$	217.65	214.51	213.0	+1.6
	$E_2 \rightarrow E_1$	217.67	214.53		
	$E_3 \rightarrow E_3$	217.67	214.53		

TABLE 6: Bending Fundamental and Torsional Hot Band Positions for Dimethylamine (cm^{-1})

$v\,v'\,v'' \rightarrow v\,v'\,v''$		MP2/TZ	MP4/TZ	obs	calc − obs
0 0 0 → 0 0 1	$A_1 \rightarrow A_1$	407.26	409.80		
	$G \rightarrow G$	407.26	409.80	383	+26.8
	$E_1 \rightarrow E_1$	407.26	409.80		
	$E_3 \rightarrow E_3$	407.26	409.80		
	gearing mode				
0 0 1 → 0 1 1	$A_1 \rightarrow A_1$	254.42	254.71		
	$G \rightarrow G$	254.37	254.71	227.6	+27.1
	$E_1 \rightarrow E_1$	254.31	254.63		
	$E_3 \rightarrow E_3$	254.31	254.63		
	antigearing mode				
0 0 1 → 1 0 1	$A_1 \rightarrow A_2$	217.24	213.43		
	$G \rightarrow G$	217.24	213.39		
	$E_1 \rightarrow E_2$	217.19	213.35		
	$E_3 \rightarrow E_3$	217.19	213.35		

(Figure 3). In contrast, in the 2D model, the barriers are constant (2412.7 and 1228.4 cm^{-1}), and the conformations corresponding to the maximum energy, the saddle-point, and minimum energy, which establish the barrier heights, exhibit different CNC angles. The 2D model barrier, however, may be compared with the average of the 3D model barrier extended to include the most probable values of β for each pair of values of the torsional angles. This average was larger than the barrier height of the 2D model barrier height and explains the displacement of the spectra.

At first sight, the 2D model barrier seems to be better than the 3D one. Indeed, the third coordinate displaces the frequencies in the wrong direction because the 2D model yields frequencies[14] that are too high. However, an enlargement of molecular basis set displaces the spectrum to lower wavenumbers. The introduction of the CNC bending coordinate and the basis set improvement have opposite effects as was also observed in DME.[17,18] Both DMA and DME analyses suggest that the electronic and nuclear calculations have to be improved simultaneously.

As expected from the G_{18} r-NRG structure, each state splits into four microstates that transform according to the A, E, E′, and G irreducible representations. Both models (2D and 3D) predict a splitting of 0.1 cm^{-1}. The G component[14] is regarded as the center of the bands.

The fundamental frequencies of the υ_{12}, υ_{24} and υ_{11} modes were determined to be 255.43, 216.86, and 409.8 cm^{-1} [MP4/6-311G(d,p)] at 0.9, 2.5, and 26.8 cm^{-1} from the experimental values,[1] respectively. The 3D model accurately reproduces the torsional band positions. It is not good enough, however, to predict the CNC bending frequencies, but a very good improvement in the relative positions of the bands of the υ_{12} and υ_{24} modes is observed. The difference between the two fundamentals has been evaluated to be 38.58 cm^{-1} [MP4/6-311G(d,p)] and 37.94 cm^{-1} [MP2/6-311G(d,p)], which is in good agreement with the experimental data (36.9 cm^{-1}). The 2D model[14] predicts a difference of 31 cm^{-1}.

The gap between the υ_{12} and υ_{24} fundamentals depends on the torsional interaction terms of the potential, as well as on the kinetic interaction term, B_{12}. At the most stable geometry, there is no kinetic interaction between the torsion and the bending modes because their displacement vectors are perpendicular. The value of B_{12} thus does not depend on the presence of the third coordinate. Thus, the differences between calculated frequencies in 2D and 3D do not depend on the kinetic terms but on the potential energy terms. The largest potential contribution arises from the A_{11}^{ss} coefficients, which are constant in the 2D model and a function of β:

$$A_{11}^{ss} = A_{110}^{ss} + A_{111}^{ss}\,\beta + A_{112}^{ss}\,\beta^2 + A_{11}^{ss}\,\beta^3$$

in the 3D model. As it was observed in DME,[17,18] accurate calculations of the $A^s{}_1s_1$ function improve the quality of the DMA fundamental frequencies. In addition, the υ_{12} frequencies depend on the potential energy function for which $\theta_1 = -\theta_2$, whereas the υ_{24} ones depend on that where $\theta_1 = \theta_2$. These steric hindrances between the two methyl hydrogen atoms may be expected to produce opposite effects in the υ_{12} and υ_{24} frequencies (gearing effects), and therefore the present calculations improve the gap between fundamentals.

The frequencies of the fundamental band, and first, second, and third sequences of the υ_{12} mode were determined to be 255.43 cm^{-1}, and 251.79, 246.97, and 240.38 cm^{-1}, respectively, which is in good agreement with the experimental data[1] (256.3 cm^{-1}, and 250.8, 245.3, and 239.8 cm^{-1}, respectively). The differences between calculated and experimental υ_{12} data obtained using the 3D model are similar to those obtained in the 2D model.[14] The calculated fundamental and first sequence of the υ_{24} bands were 216.86 and 214.51 cm^{-1}, which is in good agreement with the experimental data[1] (219.4 and 213.0 cm^{-1}, respectively).

Table 6 gives the vibrational data for the two first torsional hot bands. The present calculations are in disagreement with the assignments of Durig et al.[1] The differences could arise from the inadequacy of the 3D model or from the experimental data that were deduced from the 2D model. The exact determination of these bands would probably require to consider the effect of the NH wagging mode as observed in methylamine.[21] In DMA, a large interaction may be expected, the wagging angle (γ) is, indeed, seen to vary with the bending angle: at $\theta_1 = \theta_2 = 60°$, we have $\gamma = 60.996°$, 57.092°, and 52.522°, for $\beta = -5°$, 0°, and +5°, respectively.

Finally, it may be added that Fermi interactions between the bending and the torsional modes have not been observed. The significant improvement of the 3D model relative to the 2D model results from the proper description of the potential torsional parameters that depends on the bending angle β.

Acknowledgment. This work has been supported by the European Union under the Human Capital and Mobility Scheme (contract CHRZ CT 93-0157). The authors also acknowledge the financial assistance from the "Comision Interministerial de Ciencias y Tecnologia" of Spain through grant no. PB 93-0185. D.C.M. thanks the NSERC for financial support.

References and Notes

(1) Durig, J. R.; Griffin, M. G.; Groner, P. *J. Phys. Chem.* **1977**, *81*, 554.
(2) Aston, J. G.; Edinoff, M. L.; Forster, W. S. *J. Am. Chem. Soc.* **1939**, *61*, 1539.
(3) Barcelo, J. R.; Bellanato, J. *Spectrochim. Acta* **1956**, *8*, 27.
(4) Fateley, W. G.; Miller, F. A. *Spectrochim. Acta* **1962**, *18*, 977.
(5) Möller, K. D.; De Meo, A. R.; Smith, D. R.; London, L. H. *J. Chem. Phys.* **1967**, *47*, 2609.
(6) Dellepiane, G.; Zerbi, G. *J. Chem. Phys.* **1968**, *48*, 3573.
(7) Wollrab, J. E.; Laurie, V. W. *J. Chem. Phys.* **1968**, *48*, 5058.
(8) Wollrab, J. E.; Laurie, V. W. *J. Chem. Phys.* **1971**, *54*, 532.
(9) Gamer, G.; Wolff, H. *Spectrochim. Acta* **1973**, *29A*, 129.
(10) Smeyers, Y. G.; Huertas-Cabrera, A. *Theor. Chim. Acta* **1983**, *64*, 97.
(11) Smeyers, Y. G.; Fernandez, M.; Botella, V. J. *Mol. Struct. (Teochem)* **1990**, *210*, 273.
(12) Siam, K.; Van Alsenoy, C.; Schåfer, L. *J. Mol. Struct. (Teochem)* **1990**, *209*, 387.
(13) Consalvo, D.; van Bladel, J. W. I.; Engeln, R.; Reuss, J. *Chem. Phys.* **1993**, *171*, 221.
(14) Senent, M. L.; Smeyers, Y. G. *J. Chem. Phys.* **1996**, *105*, 2789.
(15) Smeyers, Y. G.; Senent, M. L.; Botella, V.; Moule, D. C. *J. Chem. Phys.* **1993**, *98*, 2754.
(16) Senent, M. L.; Moule, D. C.; Smeyers, Y. G.; Toro-Labbé, A.; Peñalver, F. J. *J. Mol. Spectrosc.* **1994**, *164*, 66.
(17) Senent, M. L.; Moule, D. C.; Smeyers, Y. G. *Can. J. Phys.* **1995**, *73*, 425.
(18) Senent, M. L.; Moule, D. C.; Smeyers, Y. G. *J. Chem. Phys.* **1995**, *102*, 5952.
(19) Senent, M. L.; Moule, D. C.; Smeyers, Y. G. *J. Phys. Chem.* **1995**, *99*, 7970.
(20) Senent, M. L.; Moule, D. C.; Smeyers, Y. G. *J. Mol. Struct.* **1996**, *372*, 257.
(21) Smeyers, Y. G.; Villa, M.; Senent, M. L. *J. Mol. Spectrosc.* **1996**, *177*, 66.
(22) Smeyers, Y. G. In *Advances in Quantum Chemistry*; Lowden, P. O., Ed.; Academic New York, 1992, vol 24, pp 1−77.
(23) Smeyers, Y. G. In *Structure and Dynamics of Nonrigid Molecular Systems*; Smeyers, Y. G., Ed.; Kluwer Academic: Norwell, MA, 1994.
(24) Smeyers, Y. G.; Bellido, M. N. *Int. J. Quantum. Chem.* **1981**, *19*, 553.
(25) Frisch, M. J.; Trucks, G. W.; Head-Gordon, M.; Gill, P. M. W.; Wong, M. W.; Foresman, J. B.; Johnson, B. G.; Schlegel, H. B.; Robb, M. A.; Replogle, E. S.; Gomperts, R.; Andres, J. L.; Raghavachari, K.; Binkley, J. S.; Gonzalez, C.; Martin, R. L.; Fox, D. J.; Defrees, D. J.; Baker, J.; Steward, J. J. P.; Pople, J. A. *Gaussian 92*; Gaussian, Inc.: Pittsburgh, PA, 1992.
(26) *SPSS/PC+Statistics 4.0*, SSPS Intenational BV, 1990.
(27) Harthcock, M. A.; Laane, J. *J. Phys. Chem.* **1985**, *89*, 4231.